Letter Vol. 47, No. 14 / 15 July 2022 / Optics Letters 3527

Mode-locking induced by coherent driving in fiber lasers

Carlos Mas Arabí,[1] Nicolas Englebert,[1] Pedro Parra-Rivas,[1,2] Simon-Pierre Gorza,[1] and François Leo[1]

[1]OPERA-photonics, Université libre de Bruxelles, 50 Avenue F. D. Roosevelt, CP 194/5 B-1050 Bruxelles, Belgium
[2]Dipartimento di Ingegneria dell'Informazione, Elettronica e Telecomunicazioni, Sapienza Università di Roma, via Eudossiana 18, 00184 Rome, Italy

Received 4 May 2022; revised 15 June 2022; accepted 18 June 2022; posted 21 June 2022; published 12 July 2022

Mode-locking is a broad concept that encompasses different processes enabling short optical pulse formation in lasers. It typically requires an intracavity mechanism that discriminates between single and collective mode lasing, which can be complex and sometimes adds noise. Moreover, known mode-locking schemes do not guarantee phase stability of the carrier wave. Here, we theoretically propose that injecting a detuned signal seamlessly leads to mode-locking in fiber lasers. We show that phase-locked pulses, akin to cavity solitons, exist in a wide range of parameters. In that regime the laser behaves as a passive resonator due to the non-instantaneous gain saturation.

https://doi.org/10.1364/OL.463061

Optical dissipative solitons (DSs) are pulses propagating without distortion in an optical cavity [1]. DSs belong to the wider class of dissipative localized structures which emerge in different fields such as hydrodynamics [2] or plasma physics [3]. DSs can take many shapes, depending on the parameters of the system. We focus on the dissipative counterparts of the well-known sech-shaped nonlinear Schrödinger soliton, which attracts much attention in both mode-locked lasers [4] and passive nonlinear resonators [5–7]. In the latter, they are called cavity solitons (CSs). The main difference between lasers and passive resonators lies in how the energy is provided to the system. In lasers, the gain is incoherent while in passive resonators energy comes from an external source. Coherent driving adds a control parameter through the cavity detuning, leading to bistability in Kerr resonators [8], which in turn allows for the formation of coherent solitons on a stable background [9]. In lasers, solitons are not phase-locked and they are only stable on the condition that the trivial off solution is stable in-between pulses [10], which requires active or passive mode-locking mechanisms such as intracavity modulation [11], saturable absorbers [10], and Kerr lensing [12], among others [13,14].

Here, we theoretically show that, similarly to passive resonators, an injected continuous wave (CW) signal seamlessly leads to mode-locking in fiber lasers. In connection with our recent results on soliton formation in active resonators pumped below the lasing threshold [15], we call them active cavity solitons (ACSs). ACSs exist in the regime where the saturated incoherent gain is lower than the intracavity loss. In that configuration, the laser cavity can be treated as a low-loss passive resonator. ACSs are hence intrinsically linked to CSs. They are phase-locked to a driving laser which forms a homogeneous background around the sech-shaped soliton. Phase locking of laser solitons to a CW driving signal has already been proposed [16,17], but we demonstrate that the role of an injected source goes beyond adding coherence. It induces mode-locking in the absence of standard schemes and the driving frequency can be harnessed to tune the pulse properties.

The physical system we consider is depicted in Fig. 1. It consists of a driven fiber resonator incorporating a short erbium-doped fiber amplifier. Under some conditions, in particular when the gain dynamics is much slower than the round trip time, the dimensionless slowly varying electric field envelope E and gain g can be modeled by the following normalized mean-field model:

$$\frac{\partial E(T,\tau)}{\partial T} = \left[-1 + g(T) + i(|E(T,\tau)|^2 - \Delta) - i\eta\frac{\partial^2}{\partial\tau^2}\right]E(T,\tau) + S, \tag{1}$$

$$\frac{dg(T)}{dT} = \mu[-(1 + \xi\langle|E(T,\tau)|^2\rangle)g(T) + \mathcal{G}_0], \tag{2}$$

where T is the slow time scaled with respect to the round trip time t_R; τ is time in a reference frame traveling at the carrier frequency group velocity; Δ is the normalized phase detuning; S is the normalized driving; $\mathcal{G}_0$ is the ratio between the small-signal gain and the intrinsic cavity loss; ξ is related to the saturation power; and $\mu = \alpha_i t_R/\tau_g$ where τ_g=10 ms is the erbium relaxation time. The normalized parameters are linked to physical quantities through the relations: $T \to \alpha_i T/t_R$ where α_i is equal to the total intrinsic cavity losses; $\Delta = \delta/\alpha_i$, where δ is the cavity phase detuning in physical units; $\tau \to \tau\sqrt{2\alpha_i/(|\beta_2|L)}$ where β_2 is the group velocity dispersion; $\eta = \mathrm{sign}(\beta_2)$ and L is the cavity length; $E \to E\sqrt{\gamma L/\alpha_i}$, where γ is the Kerr nonlinear coefficient, $S^2 = \frac{P_{in}\gamma L\theta}{\alpha_i^3}$ where θ is the power transmission coefficient of the coupler; $\xi = \alpha_i/(\gamma L P_{sat})$, where P_{sat} is the saturation power. The average power $\langle|E|^2\rangle$ is evaluated over one round trip [18,19]: $\langle|E|^2\rangle = t_c^{-1}\int_{-t_c/2}^{t_c/2}|E|^2 d\tau$ where $t_c = t_R\sqrt{2\alpha_i/(|\beta_2|L)}$ is the normalized round trip time. In what follows, we focus on the anomalous regime ($\eta = -1$).

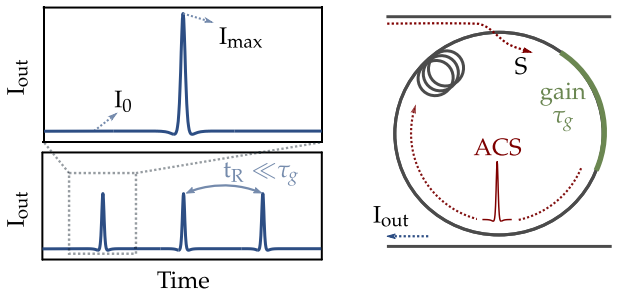

Fig. 1. Schematic representation of a coherently driven active Kerr fiber resonator. The cavity round trip time (t_R) is several orders of magnitude shorter than the gain lifetime (τ_g).

The stationary solutions of Eqs. (1) and (2) satisfy the equation

$$0 = \left[-1 + \frac{\mathcal{G}_0}{(1+\xi\langle|E(\tau)|^2\rangle)} + i(|E(\tau)|^2 - \Delta) + i\frac{\partial^2}{\partial\tau^2}\right]E(\tau) + S. \tag{3}$$

We readily note that this equation resembles the stationary Lugiato–Lefever equation (LLE) [8]. The only difference comes from the additional saturated gain term. In this work, we focus on the region where the saturated gain is lower than the intracavity loss such that the cavity behaves as a passive resonator with high effective finesse. For solitons hosted in long passive resonators, most of the optical energy stored in the resonator comes from the low-power CW background. We hence start by making the approximation $\langle|E(\tau)|^2\rangle \approx I_0$, where I_0 is the power of the CW background (see Fig. 1), to identify the regions of existence of CSs in our system. By introducing the effective loss $\alpha_{\text{eff}} = 1 - \mathcal{G}_0/(1+\xi I_0)$ in Eq. (3), one recovers the LLE describing a passive resonator with total round trip loss α_{eff} [8,20]. The oft-used dimensionless driving (S_{eff}) and detuning (Δ_{eff}) parameters of the LLE [21] can be retrieved through the relations $S_{\text{eff}} = S/\alpha_{\text{eff}}^{3/2}$ and $\Delta_{\text{eff}} = \Delta/\alpha_{\text{eff}}$, when $\alpha_{\text{eff}}>0$. For every set (S, Δ, I_0), where I_0 is a solution of

$$S^2 = I_0\left[\left(1 - \frac{\mathcal{G}_0}{1+\xi I_0}\right)^2 + (\Delta - I_0)^2\right], \tag{4}$$

we can calculate the effective LLE parameters (S_{eff}, Δ_{eff}) and predict the existence of solitons and their stability in our active system. The region of existence of solitons in the LLE is well-known [21,22]. In the ($S_{\text{eff}}, \Delta_{\text{eff}}$) space, they are located in the region bounded by the saddle-node bifurcations SN_1 and SN_2 [see Fig. 2(a)]. SN_1 marks the low CW fold of the LLE and SN_2 is the soliton saddle-node. The latter is well approximated by the expression $SN_2 = 2\alpha_{\text{eff}}\sqrt{2\Delta}/\pi$ [5,23]. The Hopf bifurcation (HB) line (calculated numerically), indicates the region where solitons lose stability and oscillatory behavior, as well as spatiotemporal dynamics, can be found [24].

As examples of trajectories in the ($S_{\text{eff}}, \Delta_{\text{eff}}$) plane, we use parameters which correspond to our recent experimental results [15]. In that configuration, the small-signal gain is lower than the intracavity loss (no lasing) and ($S_{\text{eff}}, \Delta_{\text{eff}}$) can be defined for all detunings Δ. We will then generalize the concept by showing that similar solitons emerge above the lasing threshold. Three different Δ-parametrized paths, corresponding to different saturation powers are shown in Fig. 2(a). The fixed parameters are $S = 0.4$, $\mathcal{G}_0 = 0.92$, and $t_c = 140{,}000$. For large detunings (Δ>5,

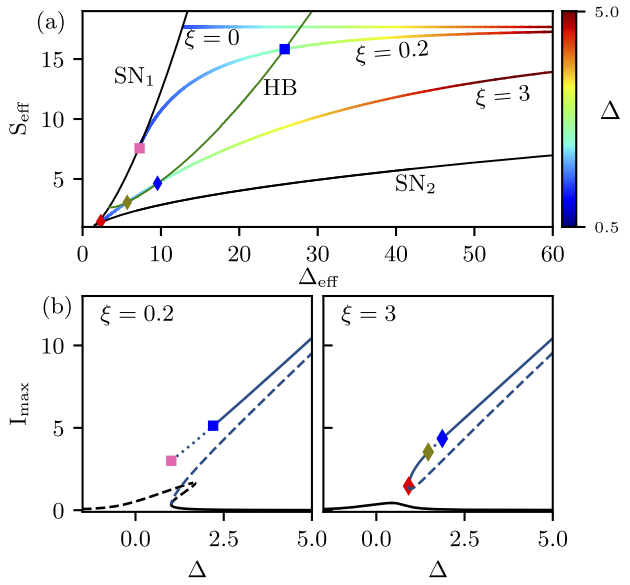

Fig. 2. (a) Phase-space ($S_{\text{eff}}, \Delta_{\text{eff}}$) of the Lugiato–Lefever equation (LLE). Soliton existence is delimited by the saddle-node bifurcations SN_1 and SN_2 (black lines). The Hopf bifurcation (HB) leading to soliton spatiotemporal oscillations is represented in green. The rainbow line shows the trajectory of our system for different saturation powers as we change the detuning Δ. (b) Soliton peak power (blue line) and power of the CW solutions (black) of the active cavity as a function of Δ. Solid, dashed, and dotted lines correspond to stable, saddle, and Hopf unstable solutions, respectively. The markers indicate the position of the corresponding crossings of bifurcation lines in panel (a). The parameters are $t_c = 140{,}000$, $\mathcal{G}_0 = 0.92$, and $S = 0.4$.

not shown), the background power I_0 is low and all trajectories (increasing Δ) asymptotically approach $S_{\text{eff}} = S/(1-\mathcal{G}_0)$, which corresponds to the normalized driving amplitude of a cavity with non-saturable gain ($\xi = 0$). Solitons are predicted to exist up to $\Delta = 30$ where $S_{\text{eff}} = 17.7$.

Below $\Delta = 5$, gain saturation impacts the effective loss and the trajectory (with decreasing Δ) bends downward. The bend depends on the saturation power. For $\xi = 0.2$, the bend is weak. The system crosses the HB, leading to oscillatory dynamics and the branch terminates at SN_1. For lower saturation powers ($\xi = 3$), the downward bend is stronger and the system crosses the bottom saddle-node SN_2, here at $S_{\text{eff}} = 1.27$, showing that a saddle and stable soliton connect for the second time. The HB line is crossed twice, indicating a smaller region with oscillatory states.

To confirm these predictions, we calculate the bifurcation structure of the full model [Eqs. (1) and (2)]. We use a standard numerical continuation algorithm (the open distribution software AUTO-07p [25]). The solutions are calculated in the domain $\tau = [0, t_c/2]$ using Neumann boundary conditions. Here, $\langle|E|^2\rangle$ is obtained through an additional integral constraint and is treated as a free parameter. The stability is calculated by computing the eigenvalues of the Jacobian matrix associated with Eqs. (1) and (2). The CW and soliton solutions corresponding to the trajectories of Fig. 2(a) are shown as a function of the detuning in Fig. 2(b).

For $\xi = 0.2$, the CW resonance is bistable, albeit on a small detuning interval and a Turing instability is present at $\Delta = -1.18$. The soliton branch emerges from the lower CW fold and is

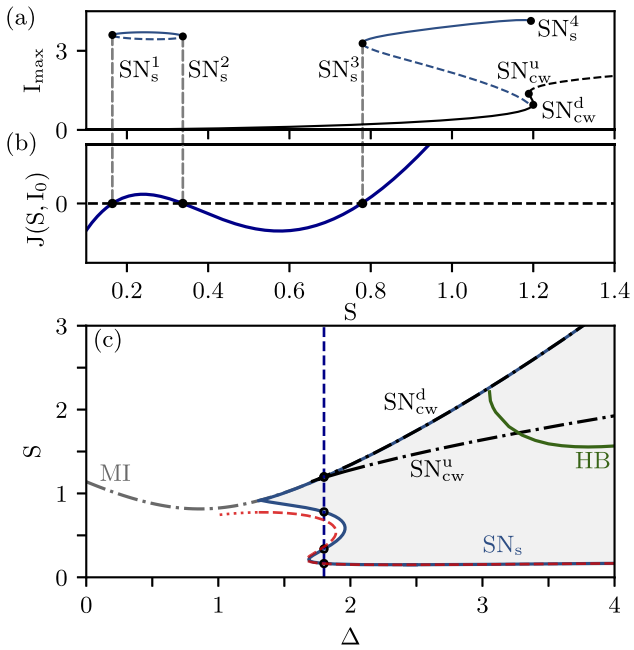

Fig. 3. (a) Soliton peak power (blue), and power of the homogeneous states (black) as a function of the driving amplitude S for $\Delta = 1.8$. (b) $J(S, I_0)$ as a function of the driving S for $\Delta = 1.8$. (c) Phase-space (Δ, S) of the system showing the soliton (blue) and homogeneous (black) saddle nodes; HB (green line). The dashed red line corresponds to the approximation $J(S, (S/\Delta)^2) = 0$ of SN_s. The parameters are $\xi = 7.75$, $\mathcal{G}_0 = 0.92$, and $t_c = 140,000$

unstable up until $\Delta = 30$ (not shown), where the stable soliton branch is created in a saddle-node bifurcation. For $\xi = 3.0$, the CW resonance is single-valued for all detunings and does not undergo modulation instability (MI) [see Fig. 2(b)]. Soliton states form two branches, one stable and the other unstable, connected on both ends by a saddle-node bifurcation (at $\Delta = 0.9$ and $\Delta = 30$, corresponding to the two crossings of SN_2). This structure is commonly called an isola [26]. The stable (top) branch undergoes two HBs at low detunings. The bifurcation structures of Fig. 2(b) are in excellent agreement with the predictions inferred from the effective LLE parameters.

We next calculate the bifurcation structure for a lower saturation power ($\xi = 7.75$). We focus on the low-detuning region, where the existence of ACSs is predicted by the condition $S_{\text{eff}} > SN_2 = 2\sqrt{2\Delta_{\text{eff}}}/\pi$, which can be written $J(I_0, \Delta) > 0$, where $J(I_0, \Delta) \equiv S - 2\alpha_{\text{eff}}\sqrt{2\Delta}/\pi$. Interestingly, at this saturation level, there is a small range of detuning where the function J possesses three zeros. This situation is shown in Fig. 3(a), where we plot the soliton branches and $J(I_0, S)$ as a function of the driving amplitude S for $\Delta = 1.8$. At low driving powers, an isola of ACSs is found, corresponding to the first two zeros of $J(I_0, S)$. The top branch of the isola is stable while the bottom one is unstable (saddle). Increasing S, we find a large parameter region without any soliton branch. A third saddle node (SN_s^3) is present around $S = 0.8$ and a stable and an unstable branch emerge again in a saddle-node bifurcation. In this case, they do not form an isola, instead the unstable branch connects with SN_{cw}^d. This latter structure is very similar to the one found in passive resonators [9]. This is because, for high background power, the gain is almost fully saturated and one recovers the bifurcation structure of the intrinsic cavity.

The two-parameter bifurcation diagram in the (S, Δ)-space for $\xi = 7.75$ is shown in Fig. 3(c). We see that the two separate regions of soliton existence connect through a necking bifurcation around $\Delta = 2$. Beyond this point, solitons exist for a very large region of parameters. Importantly, in contrast with passive resonators [22], the minimum driving amplitude necessary for soliton formation ($S > SN_s^1$) is much lower than that for Turing patterns (arising above the MI or SN_{cw}^u lines). In the region where the effective loss is low, the CW background power can be approximated by $I_0 = S^2/\Delta^2$, simplifying the evaluation of the position of SN_s. The agreement between the actual SN_s and its approximation is shown in Fig. 3(c). The threshold for soliton formation is well predicted by the approximated saddle node.

Finally, we look for connections between ACSs and laser solitons. The latter are the sech-shaped solutions of the master equation (ME) [Eq. (3) with $S = 0$] and they appear above the lasing threshold $\mathcal{G}_0 > 1$ (see, e.g., Ref. [27]). Because laser solitons are backgroundless, we reduce the normalized round trip time to $t_c = 2000$ in what follows, in order to increase the soliton-to-background energy ratio. Figure 4(a) shows a bifurcation diagram as a function of $\mathcal{G}_0$ for $\xi = 7.75$, $\Delta = 3$, and $S = 0.4$. The CW solutions are stable until $\mathcal{G}_0^H$, where the amplification exactly compensates the intrinsic cavity losses ($\alpha_{\text{eff}} = 0$). At this point, there is a HB [28], and modulated (in the slow time) solutions emerge. Further analysis of modulated solutions is beyond the scope of the present Letter. In the region $1 < \mathcal{G}_0 < \mathcal{G}_0^H$, the saturated gain is lower than the intracavity loss, which prevents lasing. This effect is commonly called injection locking and has been intensely studied in the CW regime [29,30]. In this region, the effective LLE parameters predict the existence of ACSs. Using these predictions as initial guesses, we compute the soliton solutions as a function of $\mathcal{G}_0$ for a fixed detuning and driving amplitude. The results are shown in Fig. 4(a). ACSs form two branches connected at their extremes by SN_s^a and SN_s^b. The bottom branch is always unstable, while the upper one is stable up to $\mathcal{G}_0^H$. When the detuning is small, as in Fig. 4(a), the region where stable ACSs can be found is the same as that of stable CW solutions because the gain saturation is mostly set by the CW background. For $\mathcal{G}_0 > \mathcal{G}_0^H$, the background oscillates as discussed above, and oscillatory ACSs may be found. The two ACS solutions found at $\mathcal{G}_0 = \mathcal{G}_0^H$ correspond to the well-known analytical solutions of Eq. (3) for $\alpha_{\text{eff}} = 0$ [31,32]. They read as

$$\psi_{\pm}(\tau) = \psi_0 \left[1 + \frac{2\sinh^2\beta}{1 \pm \cosh(\beta)\cosh(B\tau)} \right], \tag{5}$$

with $\psi_0 = (\Delta/(1 + 2\cosh^2\beta))^{1/2}$ and $B = (2\Delta/(1 + 2\cosh^2\beta))^{1/2}\sinh\beta$, where β is a solution of the equation $S = 2\cosh^2\beta \left[\Delta/(1 + 2\cosh^2\beta)\right]^{3/2}$.

These solutions are strongly dependent on the detuning. When the detuning is increased, the soliton peak power increases and the CW background power decreases. Here, ψ_- corresponds to the stable soliton with the maximum peak power that can be excited in our cavity for a given detuning. In Fig. 4(b), we show the evolution of the existence region of ACSs, bound by SN_s^a and ψ_-, as we change the detuning. We also show the ME (laser) soliton solutions. At large detunings, ψ_- and laser solitons asymptotically merge as the CW background of the former tends toward zero. This connection may highlight the main mechanism behind the concept of soliton injection locking. The sech-shaped solutions of the ME are phase invariant while the ψ_- has a fixed phase relation to the driving laser. Interestingly, there is a very broad region of existence of ACSs beyond these two well-known solutions. When the detuning is large, ACSs are

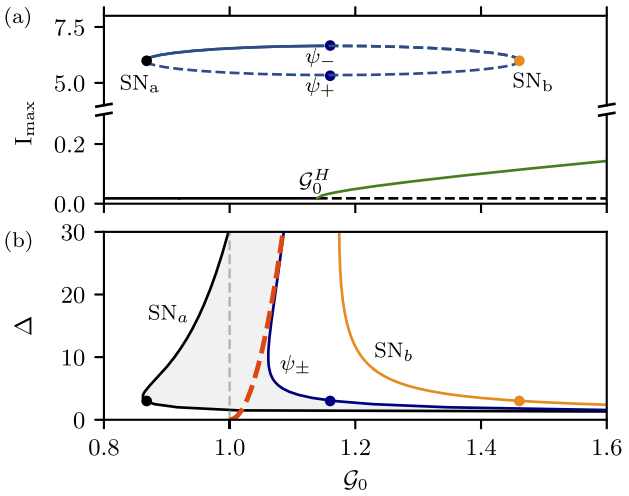

Fig. 4. (a) Soliton peak power (blue line) and CW background power (black line) as function of $\mathcal{G}_0$ for $t_c = 2000$, $S = 0.4$, $\Delta = 3.0$, and $\xi = 7.75$. Blue dots correspond to $\psi_\pm$. (b) Phase diagram in the $(\mathcal{G}_0, \Delta)$-space showing SN_s^a (black line), SN_s^b (orange line), and $\psi_\pm$ (blue line). The red line corresponds to the nonlinear phase accumulated by the ME soliton. The dashed line at $\mathcal{G}_0 = 1$ corresponds to the lasing threshold. Stable solitons exist in the gray area.

well approximated by the expression $E_{ACS} \approx \sqrt{2\Delta}\mathrm{sech}\left(\sqrt{\Delta}\tau\right)$ [21]. By changing the detuning, one can tune both the duration and the peak power of the solitons. For fixed cavity parameters and driving power, ACSs can be shorter and with higher peak power as compared with the corresponding laser soliton. Injection locking hence goes beyond fixing the phase of solitons in lasers. It induces the formation of ultra-stable solitons, with an amplitude and duration which can be externally controlled. This mode-locking process has the important advantage that it does not require an additional element such as a saturable absorber [16]. The stability of the system is guaranteed because the gain saturation is larger than the intracavity loss. Conversely, in a laser without injection, the saturated gain is equal to the intracavity loss and an additional mechanism is required to ensure the stability of the pulse in the presence of noise. Lastly, we recall that coherent driving extends the existence of solitons to regions where laser solitons do not exist, as evidenced in Fig. 4(b) by the large section of stable soliton formation that extends below $\mathcal{G}_0 = 1$ [15].

In conclusion, we showed that mode-locking can be obtained through coherent injection in fiber lasers. Stable solitons (ACSs) exist in a wide region of parameters, which extends both below and above the lasing threshold. We highlighted their connection with both solitons of passive resonators and lasers, hinting that ACSs may provide the missing link between the two. In future work, we plan to investigate ACS formation in the presence of faster gain dynamics, such as semiconductor optical amplifiers, to bridge the gap with solitons predicted in driven quantum cascade lasers [33]. Furthermore, the impact of higher-order effects, such as gain dispersion [34] or the Raman effect [35] that may affect soliton formation, especially when the injected signal is strongly detuned from resonance, will be studied.

Funding. Fonds pour la Formation à la Recherche dans l'Industrie et dans l'Agriculture; H2020 Marie Skłodowska-Curie Actions (101023717); HORIZON EUROPE European Research Council (57800); Fonds De La Recherche Scientifique - FNRS.

Disclosures. The authors declare no conflicts of interest.

Data availability. Data underlying the results presented in this paper are not publicly available at this time but may be obtained from the authors upon reasonable request.

REFERENCES

1. N. Akhmediev and A. Ankiewicz, *Dissipative Solitons, Lecture Notes in Physics* (Springer-Verlag, 2005).
2. J. Wu, R. Keolian, and I. Rudnick, Phys. Rev. Lett. **52**, 1421 (1984).
3. H. C. Kim, R. L. Stenzel, and A. Y. Wong, Phys. Rev. Lett. **33**, 886 (1974).
4. P. Grelu and N. Akhmediev, Nat. Photonics **6**, 84 (2012).
5. S. Wabnitz, Opt. Lett. **18**, 601 (1993).
6. F. Leo, S. Coen, P. Kockaert, S.-P. Gorza, P. Emplit, and M. Haelterman, Nat. Photonics **4**, 471 (2010).
7. T. Herr, V. Brasch, J. D. Jost, C. Y. Wang, N. M. Kondratiev, M. L. Gorodetsky, and T. J. Kippenberg, Nat. Photonics **8**, 145 (2014).
8. L. A. Lugiato and R. Lefever, Phys. Rev. Lett. **58**, 2209 (1987).
9. A. J. Scroggie, W. J. Firth, G. S. McDonald, M. Tlidi, R. Lefever, and L. A. Lugiato, Chaos, Solitons Fractals **4**, 1323 (1994).
10. H. A. Haus, J. Appl. Phys. **46**, 3049 (1975).
11. L. E. Hargrove, R. L. Fork, and M. A. Pollack, Appl. Phys. Lett. **5**, 4 (1964).
12. D. E. Spence, P. N. Kean, and W. Sibbett, Opt. Lett. **16**, 42 (1991).
13. L. G. Wright, D. N. Christodoulides, and F. W. Wise, Science **358**, 94 (2017).
14. H. Bao, A. Cooper, M. Rowley, L. Di Lauro, J. S. Totero Gongora, S. T. Chu, B. E. Little, G.-L. Oppo, R. Morandotti, D. J. Moss, B. Wetzel, M. Peccianti, and A. Pasquazi, Nat. Photonics **13**, 384 (2019).
15. N. Englebert, C. Mas Arabi, P. Parra-Rivas, S.-P. Gorza, and F. Leo, Nat. Photonics **15**, 536 (2021).
16. M. Margalit, M. Orenstein, and H. Haus, IEEE J. Quantum Electron. **32**, 155 (1996).
17. A. Komarov, K. Komarov, A. Niang, and F. Sanchez, Phys. Rev. A **89**, 013833 (2014).
18. A. Haboucha, H. Leblond, M. Salhi, A. Komarov, and F. Sanchez, Phys. Rev. A **78**, 043806 (2008).
19. A. Niang, F. Amrani, M. Salhi, H. Leblond, and F. Sanchez, Phys. Rev. A **92**, 033831 (2015).
20. M. Haelterman, S. Trillo, and S. Wabnitz, Opt. Commun. **93**, 343 (1992).
21. S. Coen and M. Erkintalo, Opt. Lett. **38**, 1790 (2013).
22. P. Parra-Rivas, D. Gomila, M. A. Matías, S. Coen, and L. Gelens, Phys. Rev. A **89**, 043813 (2014).
23. K. Nozaki and N. Bekki, Phys. D **21**, 381 (1986).
24. F. Leo, L. Gelens, P. Emplit, M. Haelterman, and S. Coen, Opt. Express **21**, 9180 (2013).
25. E. J. Doedel, T. F. Fairgrieve, B. Sandstede, A. R. Champneys, Y. A. Kuznetsov, and X. Wang, "AUTO-07p: Continuation and bifurcation software for ordinary differential equations,". (2007).
26. M. Beck, J. Knobloch, D. J. B. Lloyd, B. Sandstede, and T. Wagenknecht, SIAM J. Math. Anal. **41**, 936 (2009).
27. J. Kim and Y. Song, Adv. Opt. Photonics **8**, 465 (2016).
28. L. Lugiato, F. Prati, and M. Brambilla, *Nonlinear Optical Systems* (Cambridge University Press, 2015).
29. C. Buczek, R. Freiberg, and M. Skolnick, Proc. IEEE **61**, 1411 (1973).
30. J. R. Tredicce, F. T. Arecchi, G. L. Lippi, and G. P. Puccioni, J. Opt. Soc. Am. B **2**, 173 (1985).
31. I. V. Barashenkov and Y. S. Smirnov, Phys. Rev. E **54**, 5707 (1996).
32. A. B. Matsko, A. A. Savchenkov, W. Liang, V. S. Ilchenko, D. Seidel, and L. Maleki, Opt. Lett. **36**, 2845 (2011).
33. L. Columbo, M. Piccardo, F. Prati, L. A. Lugiato, M. Brambilla, A. Gatti, C. Silvestri, M. Gioannini, N. Opačak, B. Schwarz, and F. Capasso, Phys. Rev. Lett. **126**, 173903 (2021).
34. M. Haelterman, S. Trillo, and S. Wabnitz, Phys. Rev. A **47**, 2344 (1993).
35. Y. Wang, M. Anderson, S. Coen, S. G. Murdoch, and M. Erkintalo, Phys. Rev. Lett. **120**, 053902 (2018).